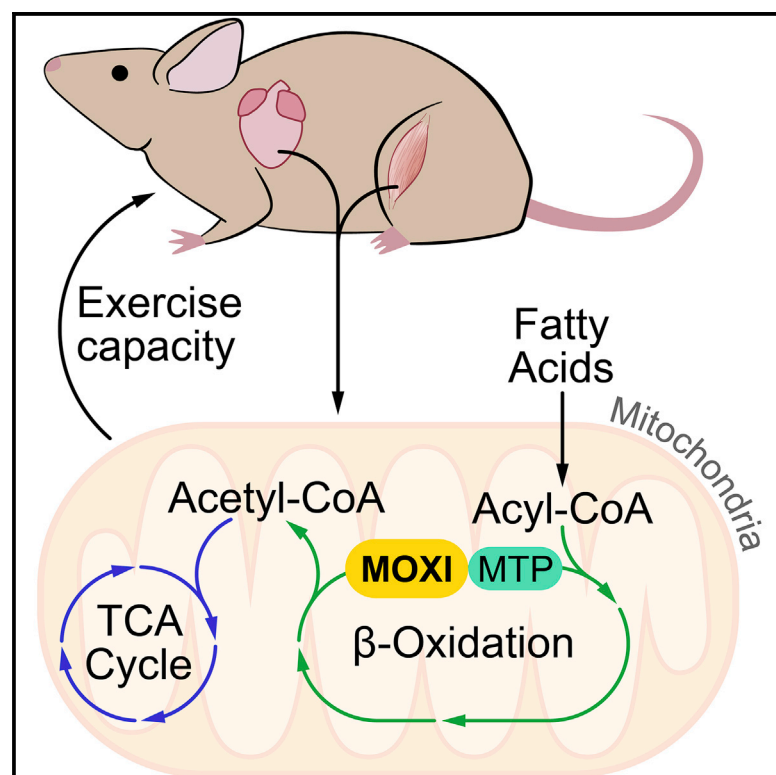# Cell Reports

MOXI Is a Mitochondrial Micropeptide That Enhances Fatty Acid β-Oxidation

Graphical Abstract

Authors

Catherine A. Makarewich,
Kedryn K. Baskin, Amir Z. Munir, ...,
Luke I. Szweda, Rhonda Bassel-Duby,
Eric N. Olson

Correspondence

eric.olson@utsouthwestern.edu

In Brief

Micropeptide regulator of β-oxidation (MOXI) is encoded by a muscle-enriched RNA transcript misannotated as non-coding. MOXI localizes to the inner mitochondrial membrane where it interacts with the trifunctional protein to modulate fatty acid β-oxidation and exercise capacity.

Highlights

- MOXI is a muscle-enriched protein encoded by an RNA that is annotated as non-coding

- MOXI interacts with the mitochondrial trifunctional protein and enhances β-oxidation

- MOXI loss- or gain-of-function in mice alters β-oxidation and substrate utilization

- MOXI knockout mice exhibit a reduced capacity for exercise

CellPress

Report

MOXI Is a Mitochondrial Micropeptide That Enhances Fatty Acid β-Oxidation

Catherine A. Makarewich,[1] Kedryn K. Baskin,[1] Amir Z. Munir,[1] Svetlana Bezprozvannaya,[1] Gaurav Sharma,[2]
Chalermchai Khemtong,[2] Akansha M. Shah,[1] John R. McAnally,[1] Craig R. Malloy,[2,3,4] Luke I. Szweda,[4]
Rhonda Bassel-Duby,[1] and Eric N. Olson[1,5,*]
[1]Department of Molecular Biology and the Hamon Center for Regenerative Science and Medicine, University of Texas Southwestern Medical
Center, Dallas, TX 75390, USA
[2]Advanced Imaging Research Center, University of Texas Southwestern Medical Center, Dallas, TX 75390, USA
[3]Department of Radiology, University of Texas Southwestern Medical Center, Dallas, TX 75390, USA
[4]Department of Internal Medicine, University of Texas Southwestern Medical Center, Dallas, TX 75390, USA
[5]Lead Contact
*Correspondence: eric.olson@utsouthwestern.edu
 https://doi.org/10.1016/j.celrep.2018.05.058

SUMMARY

Micropeptide regulator of β-oxidation (MOXI) is a conserved muscle-enriched protein encoded by an RNA transcript misannotated as non-coding. MOXI localizes to the inner mitochondrial membrane where it associates with the mitochondrial trifunctional protein, an enzyme complex that plays a critical role in fatty acid β-oxidation. Isolated heart and skeletal muscle mitochondria from MOXI knockout mice exhibit a diminished ability to metabolize fatty acids, while transgenic MOXI overexpression leads to enhanced β-oxidation. Additionally, hearts from MOXI knockout mice preferentially oxidize carbohydrates over fatty acids in an isolated perfused heart system compared to wild-type (WT) animals. MOXI knockout mice also exhibit a profound reduction in exercise capacity, highlighting the role of MOXI in metabolic control. The functional characterization of MOXI provides insight into the regulation of mitochondrial metabolism and energy homeostasis and underscores the regulatory potential of additional micropeptides that have yet to be identified.

INTRODUCTION

Advances in computational biology, transcriptome analyses, and proteomic approaches have revealed that a much larger fraction of the genome is transcribed and translated than initially recognized (Guttman et al., 2009; Ingolia et al., 2014). Notably, many small open reading frames (ORFs) that code for functional protein products have been found hidden within transcripts misannotated as non-coding (Andrews and Rothnagel, 2014; Frith et al., 2006; Mackowiak et al., 2015; Makarewich and Olson, 2017). These small proteins, or micropeptides, play essential roles in diverse biological processes, including development (Chng et al., 2013; Galindo et al., 2007; Kondo et al., 2010), DNA repair (Slavoff et al., 2014), calcium homeostasis (Anderson et al., 2015; Anderson et al., 2016; Magny et al., 2013; Nelson

et al., 2016), myoblast fusion (Bi et al., 2017), and metabolism (Lee et al., 2015).

Here, we detail our discovery and analysis of a muscle-enriched protein we termed micropeptide regulator of β-oxidation (MOXI). MOXI is a nuclear encoded peptide that localizes to the inner mitochondrial membrane (IMM), where it specifically interacts with the mitochondrial trifunctional protein (MTP), an IMM localized enzymatic complex that catalyzes the last three steps of long-chain fatty acid (LCFA) oxidation. Mitochondrial fatty acid oxidation is critical for energy homeostasis in skeletal muscle and the heart, and while the major enzymes involved in fatty acid oxidation have been identified, it is still largely unknown how these enzymes are dynamically regulated on a molecular level (Bartlett and Eaton, 2004; Lopaschuk et al., 2010; Nakamura et al., 2014; Rasmussen and Wolfe, 1999; Taegtmeyer et al., 2016). In this regard, our findings indicate that MOXI may fulfill one such role as a regulator of the MTP that helps match the metabolic demand for enhanced fatty acid oxidation in striated muscle during stress conditions.

RESULTS

MOXI Is a Conserved Muscle-Enriched Micropeptide

We discovered MOXI through a screen for putative micropeptides encoded by muscle-enriched transcripts annotated as non-coding using PhyloCSF, a comparative genomics method that identifies the evolutionarily conserved protein coding potential of genomic sequences (Lin et al., 2011). This method revealed a previously unrecognized ORF of 56 amino acids within the muscle-enriched *Moxi* transcript, annotated as *1500011K16Rik* and *LINC00116* in the mouse and human genomes, respectively. The murine *Moxi* transcript is encoded in two exons on chromosome 2 and the entire 168 base pair ORF is contained within the first exon (Figures S1A and S1B). The ORF is highly conserved across species (Figure 1A) and scores positively with PhyloCSF (Figure S1A). The N terminus of the MOXI protein is hydrophobic and is predicted to encode a transmembrane domain, whereas the C-terminal region is highly enriched in basic residues (Figure 1A).

To determine if the *Moxi* ORF is translated to a stable micropeptide, we performed *in vitro* transcription and translation

Figure 1. MOXI Is an Evolutionarily Conserved Micropeptide That Is Enriched in Muscle and Localizes to the Mitochondria

(A) Amino acid sequence alignment of vertebrate MOXI proteins. The colors of the amino acid residues indicate their properties (pink, positive charge; blue, negative charge; red, hydrophobic; green, hydrophilic). The symbols below the alignment represent the biochemical similarity of aligned amino acids with asterisks indicating identical conservation, colons representing high similarity, and periods showing somewhat similar conservation.

(B) *In vitro* transcription and translation of the full-length *Moxi* or *Pln* RNAs in the presence of radiolabeled ^{35}S-methionine. Frameshift (FS) mutations introduced within the *Moxi* and *Pln* open reading frames abolished micropeptide expression from these RNAs.

(C) Detection of *Moxi* RNA by qRT-PCR in adult mouse tissues. Quad, quadriceps; GP, gastrocnemius/plantaris; WAT, white adipose tissue; BAT, brown adipose tissue. 18S rRNA was used for normalization and expression is shown relative to liver for n = 3 mice, mean ± SD.

(D) Western blot of adult mouse tissues with a MOXI-specific antibody reveals a band at the predicted size of ∼6 kDa.

(E and F) MS/MS spectrum of two unique peptides corresponding to different regions of the MOXI protein identified by mass spectrometry on adult mouse quadriceps muscle.

(G and H) Immunofluorescence of MOXI-FLAG (green) and markers of the mitochondria (TOMM20-mCherry, red) (G) or the sarco/endoplasmic reticulum (mCherry-SERCA1, red) (H) in transfected C2C12 myoblasts. Scale bar, 5 μm.

assays using the full-length *Moxi* RNA transcript in the presence of ^{35}S-methionine (Figure 1B). A single ∼6 kilodalton (kDa) micropeptide was produced from the *Moxi* transcript, whereas a

frameshift mutation that disrupted the ORF abolished any detectable expression (Figure 1B). This pattern was identical to that of phospholamban (PLN), a similarly sized 52 amino acid

protein. Quantitative reverse transcription polymerase chain reaction (qRT-PCR) analysis revealed that *Moxi* RNA is highly abundant and enriched in striated muscle (Figure 1C). To further confirm that the *Moxi* transcript encodes a protein and validate its tissue distribution profile, we raised a polyclonal rabbit antibody against MOXI (Figure S1C). Western blot analysis confirmed that MOXI is strongly expressed in both skeletal muscle and the heart (Figure 1D). MOXI was also identified in adult mouse quadriceps muscle by mass spectrometry using in-gel elastase digestion, which produced two distinct peptide fragments of 1.1 and 1.4 kDa that correspond to unique regions of the protein (Figures 1E and 1F).

MOXI Localizes to the Inner Mitochondrial Membrane

Expression of MOXI as a C-terminal FLAG-fusion protein in C2C12 myoblasts revealed a mitochondrial distribution pattern by immunohistochemistry (Figures 1G and 1H). Co-expression of MOXI-FLAG with an mCherry-tagged mitochondrial membrane marker, translocase of outer mitochondrial membrane 20 (TOMM20), confirmed its mitochondrial localization (Figure 1G). In contrast, co-expression with the endoplasmic reticulum membrane protein sarco/endoplasmic reticulum calcium ATPase (SERCA) revealed distinct and non-overlapping patterns (Figure 1H).

MOXI contains a conserved transmembrane domain comprised of a hydrophobic core that is flanked on both sides by charged amino acid residues (Figure 1A), consistent with sequence determinants of an IMM protein (Stuart and Neupert, 1996). To assess mitochondrial membrane localization, mitochondria were isolated from adult mouse quadriceps muscle and subjected to progressive proteolysis with serial dilutions of proteinase K (PK) (Figure 2A). The outer mitochondrial membrane (OMM) protein TOMM20 was sensitive to proteolysis at much lower PK concentrations than the IMM localized α-subunit of the MTP (HADHA). Similar to HADHA, MOXI was resistant to PK proteolysis at high concentrations of PK and exhibited a degradation pattern consistent with that of an IMM protein (Figure 2A). To further validate its localization to the IMM, mitochondria from quadriceps muscle were subjected to osmotic shock to disrupt the OMM and create mitoplast fractions, which were exposed to PK proteolysis in the presence or absence of detergent (Figure 2B). MOXI exhibited a PK proteolysis resistance pattern similar to that of the IMM marker HADHA, and distinct from the OMM protein TOMM20 (Figure 2B), thus substantiating the sub-mitochondrial localization of MOXI to the IMM.

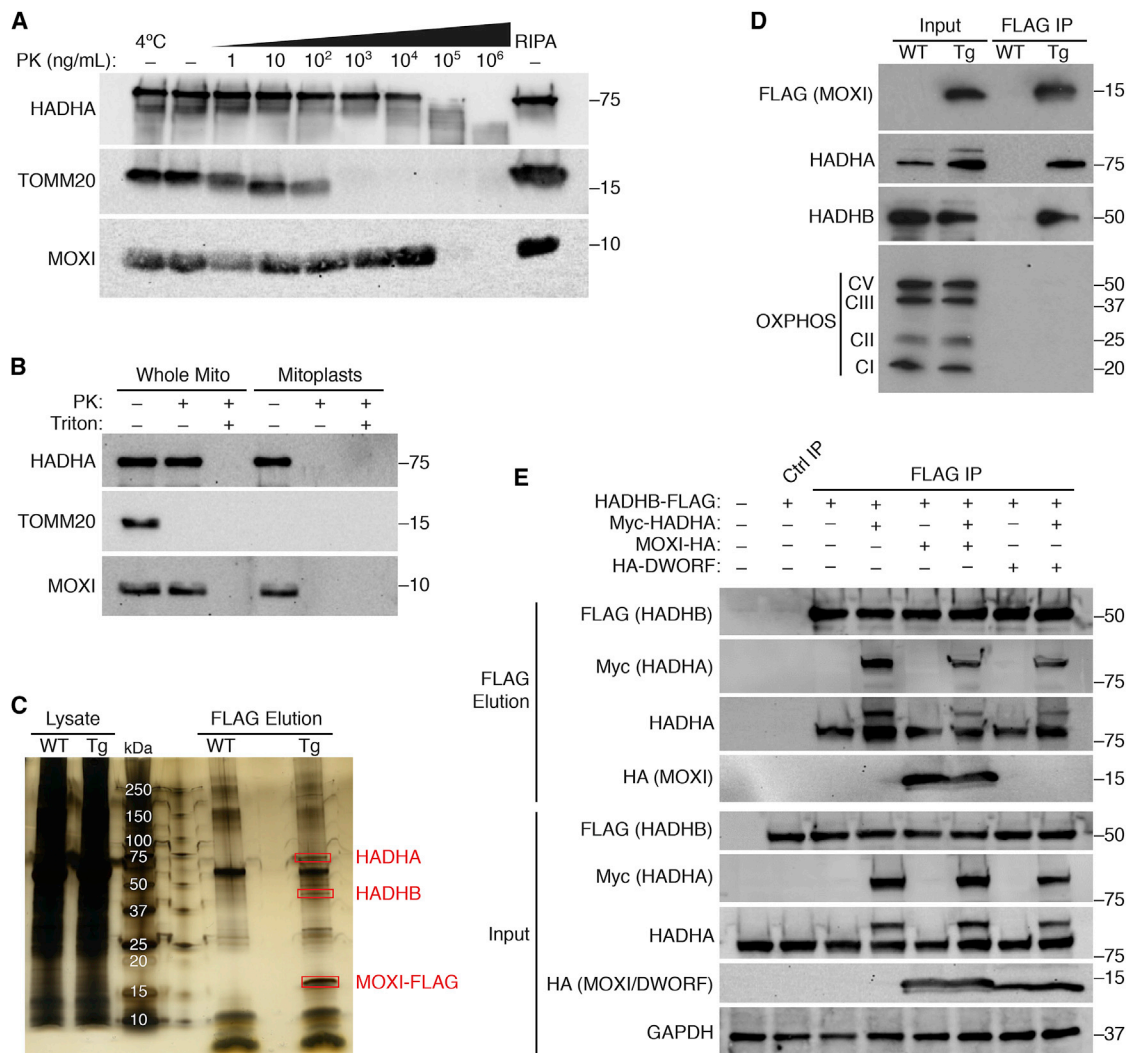## MOXI Interacts with the Mitochondrial Trifunctional Protein

To identify protein interaction partners of MOXI, we generated a transgenic (TG) mouse line with striated muscle-specific overexpression of a MOXI-FLAG fusion protein under control of the muscle creatine kinase (MCK) promoter. Proper IMM localization of MOXI-FLAG was validated before immunoprecipitation (IP) experiments were performed (Figures S2A–S2D). Quadriceps muscles of wild-type (WT) and TG mice were homogenized, and lysates were subjected to FLAG IP. Analysis of FLAG-eluted proteins by silver stain revealed three highly abundant proteins that were only present in TG samples (Figure 2C). These unique

protein bands were excised and subjected to LC-MS/MS, and peptide mass fingerprinting revealed their identity as MOXI-FLAG and the two subunits of the MTP, the α- (HADHA) and β-subunits (HADHB) (Figure 2C and Tables S1–S3). These results were validated in quadriceps tissue from WT and MOXI-FLAG TG mice by FLAG IP and western blot analysis for HADHA and HADHB (Figure 2D). The interaction of MOXI with the MTP appeared to be specific, as components of the oxidative phosphorylation (OXPHOS) complex, which are highly abundant IMM resident proteins, were excluded from the FLAG elution (Figure 2D). These results were further confirmed in gastrocnemius/plantaris muscles and in the heart of MOXI-FLAG TG mice (Figures S2E and S2F). Additionally, the interaction of MOXI and MTP was confirmed in HEK293 cells transfected with epitope-tagged versions of MOXI (HA), HADHA (Myc), and HADHB (FLAG) (Figure 2E). Cell lysates were subjected to FLAG IP, and bound proteins were eluted using FLAG peptide to purify HADHB-FLAG and its interacting partners. Western blot analysis revealed a strong association of HADHB with both endogenous untagged HADHA and transfected Myc-HADHA (Figure 2E), indicating efficient pull-down of the MTP complex. MOXI-HA was also pulled down in strong association with the MTP, while HA-DWORF, a negative control micropeptide, was not observed in the bound fraction, indicating a specific interaction between MOXI and the MTP (Figure 2E). As the MTP is a critical IMM associated protein that is essential for mitochondrial oxidation of LCFAs, we hypothesized that MOXI plays a role in regulating fatty acid oxidation.

MOXI Knockout and Transgenic Mice Exhibit Mitochondrial Abnormalities

To assess the function of MOXI *in vivo*, we generated a loss-of-function mouse model by using the clustered regularly interspaced short palindromic repeats (CRISPR)-associated protein 9 (Cas9) system to disrupt the coding frame of *Moxi*. A founder with a 1-base pair deletion and 3-base pair insertion that disrupts the ORF, resulting in premature stop codon and an unstable protein, was chosen for further analysis (Figures S3A and S3B). Heterozygous *Moxi* knockout (KO) mice yielded homozygous mutant offspring at expected Mendelian ratios. Western blot analysis of quadriceps and heart muscle performed with our MOXI-specific antibody showed that the MOXI protein was eliminated in muscle tissues of homozygous mutant KO mice (Figures 3A and 3B). Levels of MOXI overexpression in MOXI TG mice were also assessed by both western blot analysis and qRT-PCR and indicated a high level of expression of the MOXI-FLAG fusion protein, as well as an unanticipated upregulation of the endogenous MOXI protein (Figures 3A–3B and S3C–S3D). It has been demonstrated that mutations in either HADHA or HADHB can result in instability of the MTP complex and reductions in subunit expression levels (Spiekerkoetter et al., 2004a; Ushikubo et al., 1996). Therefore, we assessed whether loss of MOXI protein or its overexpression affected MTP abundance and found no changes in protein or mRNA expression levels of the α- or β-subunits (Figures 3A-3B and S3C–S3D), indicating that MOXI is not required for MTP complex formation or stability.

Compared to WT mice, both KO and TG animals had normal heart function and cardiac dimensions as assessed by
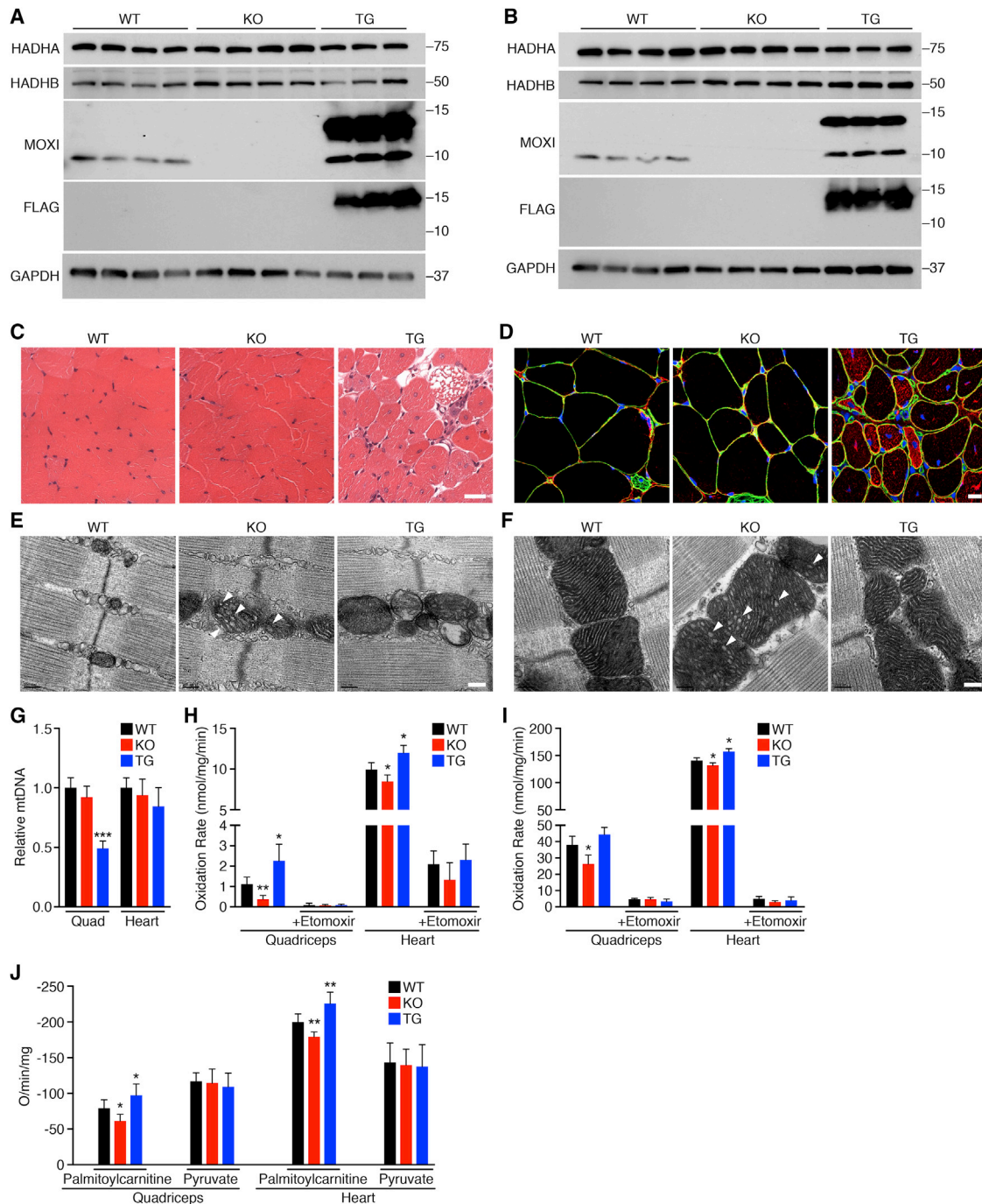
Figure 2. MOXI Localizes to the Inner Mitochondrial Membrane Where It Interacts with the Mitochondrial Trifunctional Protein

(A) Mitochondria were isolated from adult mouse quadriceps muscle and subjected to proteinase K (PK) digestion at the indicated concentrations at 37°C unless otherwise indicated. Far right, mitochondria lysed in RIPA buffer serves as a control for the total mitochondrial fraction. Western blots were performed for markers of the OMM (TOMM20), IMM (HADHA), or endogenous MOXI protein.

(B) Mouse quadriceps mitochondria were subjected to PK proteolysis to digest exposed proteins in the presence or absence of detergent (Triton). Osmotic shock was used to isolate mitoplasts, which were also subjected to PK digestion. Western blot analysis was performed using antibodies for MOXI or for the sub-mitochondrial markers HADHA and TOMM20.

(C) Silver stain analysis of FLAG immunoprecipitations (IPs) performed in mouse quadriceps muscle homogenates from wild-type (WT) or MCK-MOXI-FLAG transgenic (TG) mice. The 3 highly abundant and unique bands that are only present in the TG sample and indicated in red rectangles were analyzed by LC-MS/MS and identified as HADHA, HADHB, and MOXI-FLAG (see Tables S1–S3).

(D) Western blot analysis of FLAG IPs from quadriceps muscle homogenates of WT and MOXI-FLAG TG mice using antibodies for HADHA, HADHB, FLAG, and an OXPHOS cocktail that detects Complex I, II, III, and V of the OXPHOS complex.

(E) Co-immunoprecipitation (coIP) experiments in transfected HEK293 cells using HADHB-FLAG, Myc-HADHA and MOXI-HA or HA-DWORF. Cell lysates were immunoprecipitated using FLAG magnetic beads or a control IgG resin, and bound proteins were eluted using FLAG peptide. Proteins that were pulled down in association with HADHB-FLAG were analyzed by western blot analysis using antibodies for FLAG, Myc, HADHA, or HA. Ctrl IP, control immunoprecipitation. The HADHA antibody recognizes both the endogenous protein (lower molecular weight band) and the transfected Myc-HADHA protein (higher molecular weight band).

echocardiography (Figures S3E–S3H) and all genotypes had comparable body composition measured by EchoMRI (Figures S3I–S3K). Histologically, quadriceps sections from KO mice appeared normal, while TG animals exhibited signs of myopathy with many fibers containing centralized nuclei (Figure 3C). Addi-

tionally, degenerating muscle fibers were present throughout skeletal muscle sections of TG mice, indicating severe pathology (Figure 3C). Immunohistochemistry performed on quadriceps sections showed an accumulation of desmin in skeletal muscle fibers of TG animals, demonstrating a loss of membrane integrity

Figure 3. Consequence of MOXI Loss- and Gain-of-Function

(A and B) Western blot analysis showing the expression level of MOXI in quadriceps muscle (A) and heart (B) of WT, KO, and TG mice. The expression and stability of the MTP α-subunit (HADHA) and β-subunit (HADHB) were also analyzed.

(C) Hematoxylin and eosin (H&E) staining on quadriceps muscle sections. Scale bar, 50 μm.

(D) Immunohistochemistry on quadriceps muscle sections. Representative merged images are shown of laminin (green), desmin (red), and DAPI (blue). Scale bar, 10 μm.

(E and F) Transmission electron micrographs of quadriceps muscle (E) and heart (F) from WT, KO, and TG mice. White arrows indicate the disrupted cristae structure observed in KO mice. Representative images from n = 3 mice are shown. Scale bar, 0.2 μm.

(G) Relative mitochondrial DNA (mtDNA) content expressed as a function of total genomic DNA in quadriceps (Quad) and hearts of WT, KO, and TG mice. Data were acquired by qPCR and are represented as mean ± SD, n = 5 mice per genotype, **$p < 0.005$.

(legend continued on next page)

(Figure 3D). Succinate dehydrogenase (SDH) staining of quadriceps muscles from WT, KO, and TG mice revealed no overt differences in relative oxidative capacity among genotypes (Figure S4A); however, TG muscle fibers presented with a ragged appearance, suggesting mitochondrial abnormalities.

We assessed the ultrastructure of quadriceps muscle and heart from WT, KO, and TG mice by electron microscopy (EM) and observed unique mitochondrial abnormalities in KO and TG mice (Figures 3E–3F and S4B–S4C). KO mitochondria presented with an enlarged appearance with swollen and disrupted cristae structure in both quadriceps muscle (Figures 3E and S4B) and heart (Figures 3F and S4C). These features are consistent with previous reports from heterozygous *HADHA*^{+/−} mice that present with similar mitochondrial abnormalities (Ibdah et al., 2005; Rector et al., 2008). Additionally, EM images from TG mice reveal a clear disorganization of the mitochondrial network with regions of mitochondrial dropout that are most clearly seen in quadriceps muscle (Figures 3E and S4B) and are also present in heart sections (Figures 3F and S4C). Mitochondrial content of quadriceps and heart from WT, KO, and TG mice were assayed by mitochondrial DNA (mtDNA) content and revealed no significant difference between WT and KO animals in either tissue; however, there was a significant reduction in mtDNA content in TG quadriceps muscle (Figure 3G) that correlated with the mitochondrial dropout seen by EM in these animals (Figures 3E and S4B).

MOXI Loss-or Gain-of-Function in Mice Alters Fatty Acid β-Oxidation

To directly measure the effect of MOXI gene deletion or overexpression on LCFA oxidation, *ex vivo* palmitate oxidation was measured in isolated skeletal muscle and heart mitochondria from WT, KO, and TG mice by assessing the rate of conversion of radiolabeled palmitate into either CO_2 (Figure 3H) or acid-soluble metabolites (Figure 3I). Isolated quadriceps and heart mitochondria from KO mice exhibited a diminished ability to metabolize LCFAs compared to WT mice (Figures 3H and 3I), indicating that muscles from these animals have a lower fatty acid oxidation capacity, while TG mitochondria showed enhanced oxidation. There were no observable differences in oxidation rates in the presence of etomoxir, a potent carnitine palmitoyltransferase I (CPT-1) inhibitor, indicating similar levels of contributing non-mitochondrial oxidation between genotypes (Figures 3H and 3I).

To further assess mitochondrial function in our animals, we analyzed ADP-stimulated respiration in isolated mitochondria from quadriceps and heart tissue using either LCFAs (palmitoyl-carnitine) or pyruvate as the oxidative substrate. A significant reduction in the rate of state 3 respiration was observed in mitochondria isolated from both quadriceps and heart tissues of KO mice when palmitoylcarnitine was provided as the substrate, while no change was seen when pyruvate oxidation

was assessed (Figure 3J), indicating that respiratory function is selectively impaired for fatty acid oxidation. Conversely, palmitoylcarnitine oxidation was selectively enhanced in both skeletal muscle and heart mitochondria from TG mice, while pyruvate oxidation was unchanged (Figure 3J), once again highlighting the substrate-specific effect of MOXI overexpression on mitochondrial respiratory function.

MOXI Loss-of-Function Leads to Reduced LCFA β-Oxidation and an Intolerance to Exercise

To determine the effect of MOXI loss-of-function on substrate utilization in the heart, substrate oxidation was evaluated using ^{13}C-NMR isotopomer analysis in isolated perfused WT and KO heart preparations. TG mice were omitted from these studies due to the severe mitochondrial phenotype exhibited by these animals. Figure S4D shows the metabolism of ^{13}C-enriched substrates provided in the cardiac perfusate. Multiplet ratios in glutamate were analyzed in isolated hearts for the metabolism of $[1,6$-$^{13}C_2]$glucose, $[3$-$^{13}C]$lactate, $[3$-$^{13}C]$pyruvate, and $[U$-$^{13}C]$LCFA supplied during perfusion (Figure S4D). In this study, the labeling pattern does not allow distinction between glucose, pyruvate, and lactate oxidation, and for this reason, they are collectively termed carbohydrates. The ^{13}C multiplets from glutamate C-2 (Figure 4A), C-4 (Figure 4B), and C-3 (Figure 4C) were analyzed to evaluate substrate oxidation. KO hearts showed a decrease in C-3 and C-4 doublets with a corresponding increase in the C-2 doublet of glutamate (Figures 4A–C). ^{13}C-NMR isotopomer analysis of heart extracts from KO mice showed a decrease in LCFA oxidation and a corresponding increase in carbohydrate oxidation compared to WT hearts (Figures 4D and 4E), demonstrating that KO hearts oxidized significantly more carbohydrates than fatty acids for energy production (Figure 4E). TCA cycle flux (Figure 4F), coronary flow rate (Figure S4E), and oxygen consumption rate (Figure S4F) measured under the metabolic steady state were not significantly different between groups. Consistent with our previous results showing that mitochondria from MOXI KO mice have an impaired fatty acid oxidation capacity, these data show that functioning hearts from KO mice preferentially oxidize carbohydrates over fatty acids as substrates.

β-oxidation is a key metabolic pathway for energy homeostasis during physiological stresses such as exercise when glucose supply becomes limited and several fatty acid oxidation disorders are associated with exercise intolerance (Rinaldo et al., 2002; Spiekerkoetter et al., 2004b; Spiekerkoetter et al., 2005; Spiekerkoetter and Wood, 2010). Therefore, we examined the response of MOXI KO mice to forced treadmill running to assess their ability to respond to physical exercise. KO mice showed a significant reduction in exercise capacity as compared to WT mice and exhibited signs of exhaustion after running only half the distance and time of WT mice (Figures 4G and 4H). WT

(H and I) Fatty acid oxidation was measured by incubation of quadriceps or heart mitochondria from WT, KO, and TG mice with [^{14}C]-palmitate. Oxidation rates were determined by analyzing captured CO_2 (H) and acid soluble metabolites (ASM) (I). Where indicated, the CPT-1 inhibitor etomoxir (40 μM) was used. Data are represented as mean ± SD, n = 8 for WT and KO and n = 6 for TG. *p < 0.05, **p < 0.01.

(J) Oxygen (O) consumption rates were measured in isolated mitochondria from WT, KO, and TG mice using 1 mM malate and either palmitoylcarnitine (25 μM for heart, 50 μM for quad) or pyruvate (100 μM) as metabolic substrates. State 3 respiration was initiated with the addition of ADP at a final concentration of 0.25 mM. Data are presented as mean ± SD, n = 6 per genotype. *p < 0.05, **p < 0.01.
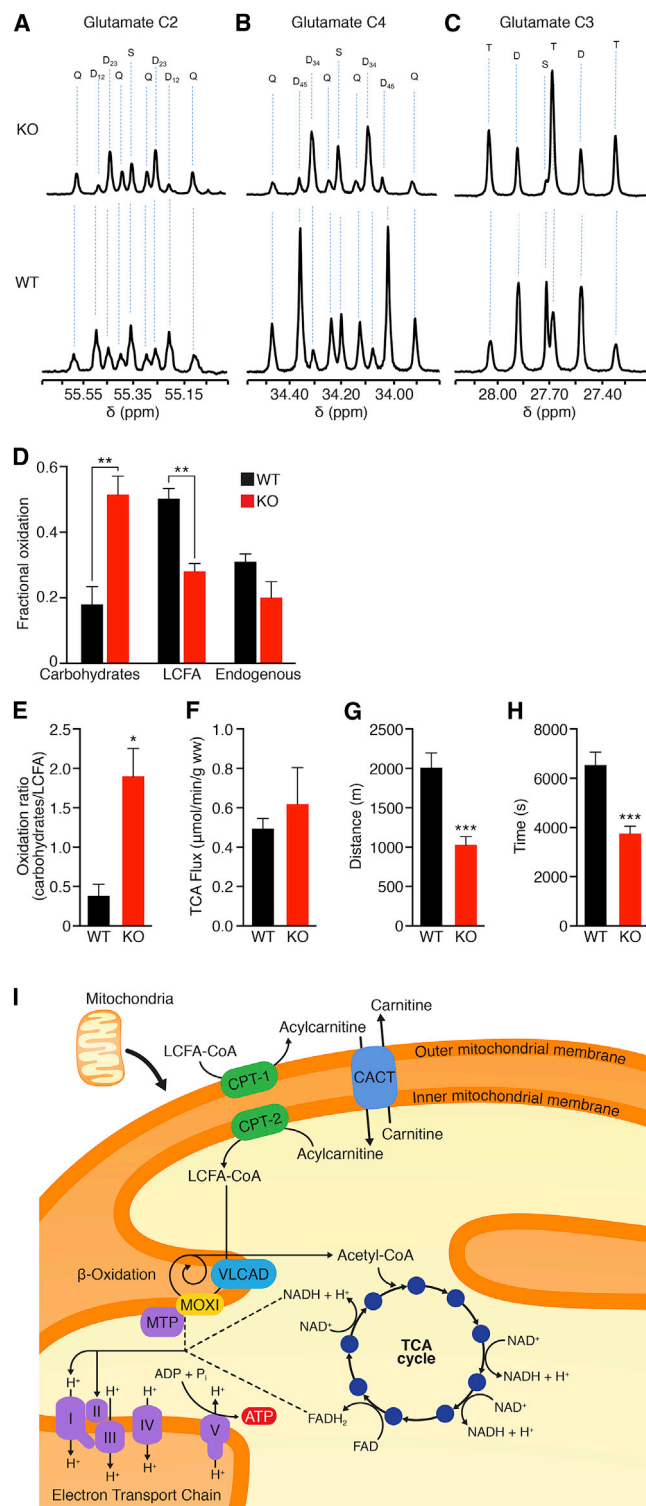
Figure 4. ¹³C-NMR Isotopomer Analysis in WT and KO Hearts and Response of KO Mice to Exercise

(A–F) Substrate oxidation was evaluated using ¹³C-NMR isotopomer analysis in isolated hearts from WT and KO mice perfused with ¹³C-labeled LCFA and carbohydrate substrates. Glutamate C-2 (55.35 ppm) (A), C-4 (34.20 ppm) (B), and C-3 (27.60 ppm) (C) spectra. The letters S, D, T, and Q refer to a singlet,

and KO mice did not lose significant weight during this acute bout of exercise, and there were no differences in blood lactate levels between groups before or after exercise (Figures S4G and S4H). These results further underscore the important role of MOXI in fatty acid oxidation and its requirement for maintaining energy homeostasis during increased metabolic demand (Figure 4I).

DISCUSSION

Fatty acids are a major fuel source required to sustain contractile function in skeletal muscle and the heart, and while the major enzymes involved in β-oxidation have been identified, the precise manner in which they are regulated is still unknown (Bartlett and Eaton, 2004; Lopaschuk et al., 2010; Nakamura et al., 2014; Rasmussen and Wolfe, 1999; Taegtmeyer et al., 2016). Here, we identify MOXI as a muscle-enriched micropeptide that interacts with the MTP in the mitochondrial inner membrane and enhances fatty acid oxidation (Figure 4I), which is required to convert the energy stored in fats into ATP. The importance of MOXI as a regulator of fatty acid oxidation is demonstrated in our loss-of-function studies where hearts from MOXI KO mice switch from using fatty acids to carbohydrates as their preferred substrate (Figures 4A–4E). The discovery of MOXI as a micropeptide capable of enhancing fatty acid oxidation through its interaction with the MTP provides insights into the complex process of metabolic control and suggests that the enzyme complexes involved in β-oxidation may be regulated by interactions with small regulatory proteins that have yet to be discovered.

In humans, fatty acid oxidation disorders present as a variety of clinical phenotypes and can result in severe disease during the early stages of life due to limited glycogen stores and a high metabolic rate that relies heavily on fatty acid oxidation for energy (Nsiah-Sefaa and McKenzie, 2016). In late-onset β-oxidation disease, symptoms can include skeletal muscle myopathies and exercise intolerance, cardiovascular disease, and neuropathy (Kompare and Rizzo, 2008). Depending on the gene affected and the exact mutation observed, the severity of fatty acid oxidation disorders varies immensely. Similar to several other gene mutations linked to β-oxidation disorders

---

doublet (with the relevant J-coupled spins), triplet (a degenerate doublet of doublets), or Q (quartet or doublet of doublets). Fractional oxidation (D), carbohydrate to long-chain fatty acid oxidation ratio (E), and TCA flux (F) were assessed for n = 4 mice per genotype. Data are presented as mean ± SEM with significance indicated as *p < 0.05, **p < 0.01.

(G and H) Exercise capacity was measured using forced treadmill running to exhaustion. MOXI KO mice ran ∼49% less distance (G) and time (H) than WT littermate controls (n = 14). Data are represented as mean ± SD ***p < 0.005.

(I) Working model for MOXI function. LCFAs are converted from acyl-CoA molecules into acylcarnitines by carnitine palmitoyltransferase 1 (CPT-1) and shuttled across the mitochondrial membrane by the carnitine-acylcarnitine translocase (CACT) where they are converted back to LCFA-CoA molecules by carnitine palmitoyltransferase 2 (CPT-2). LCFA-CoAs are metabolized by the inner membrane bound enzymes very long chain acyl-CoA dehydrogenase (VLCAD) and the mitochondrial trifunctional protein (MTP)/MOXI complex to generate acetyl-CoA molecules that then enter the TCA cycle for production of ATP and reducing coenzymes such as NADH and FADH₂. These reducing coenzymes can then be utilized by the electron transport chain to produce additional ATP.

(Cox et al., 2001; Spiekerkoetter et al., 2004b; Spiekerkoetter et al., 2005; Spiekerkoetter and Wood, 2010), no overt phenotype is observed in a loss-of-function MOXI mouse model at rest; however, when challenged with physiological stress such as exercise, MOXI KO mice fail to maintain metabolic homeostasis. There is still a great deal to be learned about how MOXI exerts its dynamic control on the MTP complex, and elucidating the precise mechanism by which it induces its effect will be the focus of future work.

In summary, the discovery of MOXI highlights the role of a previously overlooked small protein in regulating fatty acid oxidation and metabolic responsiveness. Similar to other recently discovered micropeptides (Anderson et al., 2015; Anderson et al., 2016; Nelson et al., 2016), MOXI appears to exert its biological activity by engaging with and modulating a much larger protein complex. The small size of MOXI and its distinct amino acid sequence likely contribute to its capacity to fine-tune the activity of the MTP and regulate such a complex biological system. Furthermore, our findings underscore the likelihood that additional transcripts currently classified as non-coding are misannotated and contain small ORFs that encode functional proteins. These micropeptides could serve as critical regulators of essential biological processes, and the prospect of identifying these proteins provides exciting opportunites for future discoveries.

EXPERIMENTAL PROCEDURES

Additional details and resources used in this work can be found in Supplemental Experimental Procedures.

Animals

All animal work described in this manuscript has been approved and conducted under the oversight of the UT Southwestern Institutional Animal Care and Use Committee. All mouse lines were generated on a pure C57BL/6N background. All functional experiments were performed using 12- to 16-week-old male mice.

MOXI Antibody Production

A custom polyclonal antibody was derived against the predicted MOXI protein by New England Peptide. Rabbits were immunized with a synthetic peptide with the following sequence: RYLDWRKRRLQDKL. Sera were collected and affinity purified against the peptide immunogen.

Mitochondrial Isolations for Functional Analysis

Tissues were homogenized in ice cold isolation buffer (10 mM MOPS, 210 mM mannitol, 70 mM sucrose, and 1 mM EDTA, pH 7.4). Mitochondria were resuspended in isolation buffer for mitochondrial respiratory function analysis or STE buffer (250 mM sucrose, 10 mM Tris-HCl, 1 mM EDTA, pH 7.4) for fatty acid oxidation assays. Additional information can be found in Supplemental Experimental Procedures.

Long-Chain Fatty Acid Oxidation Assays

Isolated mitochondria were incubated in oxidation reaction buffer (100 mM sucrose, 10 mM Tris-HCl, 5 mM KH_2PO_4, 0.2 mM EDTA, 80 mM KCl, 1 mM $MgCl_2$, 2 mM L-carnitine, 0.1 mM malate, 0.05 mM coenzyme A, 2 mM ATP, 1 mM DTT, and 0.7% BSA/0.1 mM palmitate/0.4 μCi ^{14}C-palmitate) for 1 hr then transferred to tubes containing 1 M perchloric acid. Fully oxidized CO_2 was captured on Whatman filter paper discs treated with 1 M NaOH and acid-soluble metabolites (ASMs) were analyzed by scintillation counting. Additional details can be found in Supplemental Experimental Procedures.

Mitochondrial Respiratory Function Analysis

Isolated heart mitochondria were diluted to 0.25 mg/mL (heart) or 0.5 mg/mL (quadriceps) in respiratory buffer composed of 10 mM MOPS, 210 mM mannitol, 70 mM sucrose, and 5 mM K_2HPO_4 at pH 7.4 and incubated with the indicated substrates. For measurements with quadriceps mitochondria, 1.25 mM $MgCl_2$ was also included in the respiratory buffer. State 3 respiration was initiated after 2 min with ADP at a final concentration of 0.25 mM. Rates of mitochondrial respiration were evaluated using a Neofox oxygen chamber. Detailed information can be found in Supplemental Experimental Procedures.

^{13}C-NMR Isotopomer Analysis

Hearts were cannulated via aorta and perfused for 30 min at 100 cm H_2O pressure at 37°C with a modified Krebs-Henseleit (KH) buffer containing 8 mM [1,6-^{13}C]glucose, 1.2 mM [3-^{13}C]lactate, 0.12 mM [3-^{13}C]pyruvate, 0.4 mM [U-^{13}C]long-chain fatty acids (LCFA), 0.75% bovine serum albumin (BSA), and 2.5 mM $CaCl_2$ equilibrated with 95:5 O_2:CO_2. After 30 min of perfusion, hearts were snap-frozen in liquid nitrogen. Proton-decoupled ^{13}C-NMR spectra of heart extracts were acquired at 600 MHz spectrometer (Bruker Corporation, USA) equipped with 5 mm cryoprobe. Additional information can be found in Supplemental Experimental Procedures.

Treadmill Exercise

Mice were run on Exer-3/6 treadmill apparatus (Columbus Instruments) with mild electrical stimulus. The treadmill was set to ramp from 0 to 10 m/min over a period of 5 min and then stay at 10 m/min for an additional 5 min. The treadmill speed then incrementally increased (1 m/min every 5 min) to a maximum speed of 20 m/min until exhaustion. Exhaustion was defined by failure to run for greater than 10 s.

Quantification and Statistical Analysis

Statistical comparisons between groups were evaluated by Student's t test using Prism 6 (GraphPad). Data are presented as mean ± SD or SEM as indicated in each figure legend. Statistical significance is denoted as *p < 0.05, **p < 0.01, ***p < 0.005, and ****p < 0.001; n indicates the number of biological replicates within each group.

SUPPLEMENTAL INFORMATION

Supplemental Information includes Supplemental Experimental Procedures, four figures, and three tables, and can be found with this article online at https://doi.org/10.1016/j.celrep.2018.05.058.

AUTHOR CONTRIBUTIONS

Conceptualization, C.A.M., K.K.B., A.Z.M., C.R.M., L.I.S., and E.N.O.; Methodology, C.A.M., A.Z.M., K.K.B., S.B., A.M.S., J.R.M., G.S., and C.K.; Visualization, C.A.M., K.K.B., and A.Z.M.; Writing, C.A.M., R.B.D., and E.N.O., Supervision, C.R.M., L.I.S., R.B.D., and E.N.O.; Project Administration, C.A.M. and R.B.D.; Funding Acquisition, C.A.M., K.K.B., C.R.M., L.I.S., R.B.D., and E.N.O.

DECLARATION OF INTERESTS

The authors declare no competing interests.

REFERENCES

Anderson, D.M., Anderson, K.M., Chang, C.L., Makarewich, C.A., Nelson, B.R., McAnally, J.R., Kasaragod, P., Shelton, J.M., Liou, J., Bassel-Duby, R., and Olson, E.N. (2015). A micropeptide encoded by a putative long noncoding RNA regulates muscle performance. Cell 160, 595–606.

Anderson, D.M., Makarewich, C.A., Anderson, K.M., Shelton, J.M., Bezprozvannaya, S., Bassel-Duby, R., and Olson, E.N. (2016). Widespread control of calcium signaling by a family of SERCA-inhibiting micropeptides. Sci. Signal. 9, ra119.

Andrews, S.J., and Rothnagel, J.A. (2014). Emerging evidence for functional peptides encoded by short open reading frames. Nat. Rev. Genet. 15, 193–204.

Bartlett, K., and Eaton, S. (2004). Mitochondrial beta-oxidation. Eur. J. Biochem. 271, 462–469.

Bi, P., Ramirez-Martinez, A., Li, H., Cannavino, J., McAnally, J.R., Shelton, J.M., Sánchez-Ortiz, E., Bassel-Duby, R., and Olson, E.N. (2017). Control of muscle formation by the fusogenic micropeptide myomixer. Science 356, 323–327.

Chng, S.C., Ho, L., Tian, J., and Reversade, B. (2013). ELABELA: a hormone essential for heart development signals via the apelin receptor. Dev. Cell 27, 672–680.

Cox, K.B., Hamm, D.A., Millington, D.S., Matern, D., Vockley, J., Rinaldo, P., Pinkert, C.A., Rhead, W.J., Lindsey, J.R., and Wood, P.A. (2001). Gestational, pathologic and biochemical differences between very long-chain acyl-CoA dehydrogenase deficiency and long-chain acyl-CoA dehydrogenase deficiency in the mouse. Hum. Mol. Genet. 10, 2069–2077.

Frith, M.C., Forrest, A.R., Nourbakhsh, E., Pang, K.C., Kai, C., Kawai, J., Carninci, P., Hayashizaki, Y., Bailey, T.L., and Grimmond, S.M. (2006). The abundance of short proteins in the mammalian proteome. PLoS Genet. 2, e52.

Galindo, M.I., Pueyo, J.I., Fouix, S., Bishop, S.A., and Couso, J.P. (2007). Peptides encoded by short ORFs control development and define a new eukaryotic gene family. PLoS Biol. 5, e106.

Guttman, M., Amit, I., Garber, M., French, C., Lin, M.F., Feldser, D., Huarte, M., Zuk, O., Carey, B.W., Cassady, J.P., et al. (2009). Chromatin signature reveals over a thousand highly conserved large non-coding RNAs in mammals. Nature 458, 223–227.

Ibdah, J.A., Perlegas, P., Zhao, Y., Angdisen, J., Borgerink, H., Shadoan, M.K., Wagner, J.D., Matern, D., Rinaldo, P., and Cline, J.M. (2005). Mice heterozygous for a defect in mitochondrial trifunctional protein develop hepatic steatosis and insulin resistance. Gastroenterology 128, 1381–1390.

Ingolia, N.T., Brar, G.A., Stern-Ginossar, N., Harris, M.S., Talhouarne, G.J., Jackson, S.E., Wills, M.R., and Weissman, J.S. (2014). Ribosome profiling reveals pervasive translation outside of annotated protein-coding genes. Cell Rep. 8, 1365–1379.

Kompare, M., and Rizzo, W.B. (2008). Mitochondrial fatty-acid oxidation disorders. Semin. Pediatr. Neurol. 15, 140–149.

Kondo, T., Plaza, S., Zanet, J., Benrabah, E., Valenti, P., Hashimoto, Y., Kobayashi, S., Payre, F., and Kageyama, Y. (2010). Small peptides switch the transcriptional activity of Shavenbaby during Drosophila embryogenesis. Science 329, 336–339.

Lee, C., Zeng, J., Drew, B.G., Sallam, T., Martin-Montalvo, A., Wan, J., Kim, S.J., Mehta, H., Hevener, A.L., de Cabo, R., and Cohen, P. (2015). The mitochondrial-derived peptide MOTS-c promotes metabolic homeostasis and reduces obesity and insulin resistance. Cell Metab. 21, 443–454.

Lin, M.F., Jungreis, I., and Kellis, M. (2011). PhyloCSF: a comparative genomics method to distinguish protein coding and non-coding regions. Bioinformatics 27, i275–i282.

Lopaschuk, G.D., Ussher, J.R., Folmes, C.D., Jaswal, J.S., and Stanley, W.C. (2010). Myocardial fatty acid metabolism in health and disease. Physiol. Rev. 90, 207–258.

Mackowiak, S.D., Zauber, H., Bielow, C., Thiel, D., Kutz, K., Calviello, L., Mastrobuoni, G., Rajewsky, N., Kempa, S., Selbach, M., and Obermayer, B. (2015). Extensive identification and analysis of conserved small ORFs in animals. Genome Biol. 16, 179.

Magny, E.G., Pueyo, J.I., Pearl, F.M., Cespedes, M.A., Niven, J.E., Bishop, S.A., and Couso, J.P. (2013). Conserved regulation of cardiac calcium uptake by peptides encoded in small open reading frames. Science 341, 1116–1120.

Makarewich, C.A., and Olson, E.N. (2017). Mining for Micropeptides. Trends Cell Biol. 27, 685–696.

Nakamura, M.T., Yudell, B.E., and Loor, J.J. (2014). Regulation of energy metabolism by long-chain fatty acids. Prog. Lipid Res. 53, 124–144.

Nelson, B.R., Makarewich, C.A., Anderson, D.M., Winders, B.R., Troupes, C.D., Wu, F., Reese, A.L., McAnally, J.R., Chen, X., Kavalali, E.T., et al. (2016). A peptide encoded by a transcript annotated as long noncoding RNA enhances SERCA activity in muscle. Science 351, 271–275.

Nsiah-Sefaa, A., and McKenzie, M. (2016). Combined defects in oxidative phosphorylation and fatty acid β-oxidation in mitochondrial disease. Biosci. Rep. 36, e00313.

Rasmussen, B.B., and Wolfe, R.R. (1999). Regulation of fatty acid oxidation in skeletal muscle. Annu. Rev. Nutr. 19, 463–484.

Rector, R.S., Payne, R.M., and Ibdah, J.A. (2008). Mitochondrial trifunctional protein defects: clinical implications and therapeutic approaches. Adv. Drug Deliv. Rev. 60, 1488–1496.

Rinaldo, P., Matern, D., and Bennett, M.J. (2002). Fatty acid oxidation disorders. Annu. Rev. Physiol. 64, 477–502.

Slavoff, S.A., Heo, J., Budnik, B.A., Hanakahi, L.A., and Saghatelian, A. (2014). A human short open reading frame (sORF)-encoded polypeptide that stimulates DNA end joining. J. Biol. Chem. 289, 10950–10957.

Spiekerkoetter, U., and Wood, P.A. (2010). Mitochondrial fatty acid oxidation disorders: pathophysiological studies in mouse models. J. Inherit. Metab. Dis. 33, 539–546.

Spiekerkoetter, U., Khuchua, Z., Yue, Z., Bennett, M.J., and Strauss, A.W. (2004a). General mitochondrial trifunctional protein (TFP) deficiency as a result of either alpha- or beta-subunit mutations exhibits similar phenotypes because mutations in either subunit alter TFP complex expression and subunit turnover. Pediatr. Res. 55, 190–196.

Spiekerkoetter, U., Tokunaga, C., Wendel, U., Mayatepek, E., Exil, V., Duran, M., Wijburg, F.A., Wanders, R.J., and Strauss, A.W. (2004b). Changes in blood carnitine and acylcarnitine profiles of very long-chain acyl-CoA dehydrogenase-deficient mice subjected to stress. Eur. J. Clin. Invest. 34, 191–196.

Spiekerkoetter, U., Tokunaga, C., Wendel, U., Mayatepek, E., Ijlst, L., Vaz, F.M., van Vlies, N., Overmars, H., Duran, M., Wijburg, F.A., et al. (2005). Tissue carnitine homeostasis in very-long-chain acyl-CoA dehydrogenase-deficient mice. Pediatr. Res. 57, 760–764.

Stuart, R.A., and Neupert, W. (1996). Topogenesis of inner membrane proteins of mitochondria. Trends Biochem. Sci. 21, 261–267.

Taegtmeyer, H., Young, M.E., Lopaschuk, G.D., Abel, E.D., Brunengraber, H., Darley-Usmar, V., Des Rosiers, C., Gersztenn, R., Glatz, J.F., Griffin, J.L., et al.; American Heart Association Council on Basic Cardiovascular Sciences (2016). Assessing Cardiac Metabolism: A Scientific Statement From the American Heart Association. Circ. Res. 118, 1659–1701.

Ushikubo, S., Aoyama, T., Kamijo, T., Wanders, R.J., Rinaldo, P., Vockley, J., and Hashimoto, T. (1996). Molecular characterization of mitochondrial trifunctional protein deficiency: formation of the enzyme complex is important for stabilization of both alpha- and beta-subunits. Am. J. Hum. Genet. 58, 979–988.